Available online at www.sciencedirect.com
ScienceDirect
Journal of Sound and Vibration 320 (2009) 838–858
JOURNAL OF SOUND AND VIBRATION
www.elsevier.com/locate/jsvi

Direct numerical simulations of tonal noise generated by laminar flow past airfoils

R.D. Sandberg[a,*], L.E. Jones[a], N.D. Sandham[a], P.F. Joseph[b]

[a]*Aerodynamics and Flight Mechanics Research Group, School of Engineering Sciences, University of Southampton, Southampton SO17 1BJ, UK*
[b]*Institute of Sound and Vibration Research, University of Southampton, Southampton SO17 1BJ, UK*

Received 23 January 2008; received in revised form 3 September 2008; accepted 3 September 2008
Handling Editor: C.L. Morfey
Available online 11 October 2008

Abstract

A numerical investigation is presented of noise generated by flow past symmetric NACA airfoils with different thickness and at various angles of attack at $M = 0.4$ and a Reynolds number based on chord of $Re = 50,000$. Direct numerical simulations (DNS) are employed to directly compute both the near-field hydrodynamics and the far-field sound. The DNS data are then used to investigate whether the approach of determining tonal noise radiation based on the surface pressure difference, as done in the classical trailing-edge theory of Amiet, yields satisfactory results for finite thickness airfoils subject to mean loading effects. In addition, the accuracy of Amiet's surface pressure jump function is evaluated. Overall, the modified theory of Amiet appears to be suitable for finite thickness airfoils up to moderate incidence. However, when increasing the airfoil thickness to 12% chord, which corresponds to a trailing-edge angle of 16.8°, an unexpected phase change between the incident and scattered pressure is found at the frequency of the forced instability waves. This phase change is attributed to the flow oscillating around the trailing edge at a separate wake frequency. For the largest incidence investigated, Amiet's response function does not predict the total surface pressure difference as accurately as for zero or small incidence at the vortex shedding frequency, resulting in a poor prediction of the directivity and amplitude of the acoustic pressure. Moreover, predicting the airfoil self-noise based on the surface pressure difference appears not to be generally applicable at higher angles of attack because the radiated sound is only partly due to classical trailing-edge noise mechanisms. In these cases, it appears as if volume sources in the flow cannot be neglected.

1. Introduction

In most applications, airfoils are subject to unsteady pressure disturbances, caused by incident gusts, an unsteady wake, or turbulent boundary layer flows, to name a few. When the pressure fluctuations encounter a sharp edge of a solid body, a scattering process occurs which leads to a considerable increase in the radiated sound power (M^5-scaling [1]) compared with radiation in free space (M^8-scaling [2,3]). For that reason, trailing-edge noise can be considered to be one of the main sources of sound in flows over airfoils, in particular

*Corresponding author. Tel.: +44 23 80597386.
E-mail address: sandberg@soton.ac.uk (R.D. Sandberg).

0022-460X/$ - see front matter © 2008 Elsevier Ltd. All rights reserved.
doi:10.1016/j.jsv.2008.09.003

Nomenclature

A_{dist}	amplitude of disturbance
b	semi-chord
c	speed of sound
E	total energy $E = T/[\gamma(\gamma-1)M^2] + 0.5u_iu_i$
E^*	Fresnel integral
f_i	scaling of incident pressure field
F_i	forcing term
$H_1^{(2)}$	first-order Hankel function of the second kind
H_D, H_S	surface pressure jump transfer function
K_x	non-dimensional wavenumber $K_x = \omega b/U_c$
M	Mach number
p	pressure
Pr	Prandtl number
q_k	heat-flux vector
R	$\sqrt{(y_1-x_1)^2+\beta^2(y_2-x_2)^2}$
R_d	$\sqrt{x_1^2+x_2^2}$
Re	Reynolds number
t	time
T	temperature
u_i	velocity vector
U, U_c	streamwise freestream velocity, convection speed
x_i, y_i	coordinates normalized with b

Greek letters

β	$\sqrt{1-M^2}$
γ	ratio of specific heats
Δp	pressure difference between top and bottom surface
ε	convergence factor
μ	molecular viscosity
μ_0	reduced frequency $\mu_0 = \omega b/(c\beta^2)$
ρ	density
τ_{ik}	stress tensor
ω	frequency

Subscripts

$1,2$	indices for streamwise and wall-normal directions
i	incident
i,j,k	indices for Cartesian tensor notation
s	scattered
t	total

for low Mach numbers. Several theories of trailing-edge noise have been developed relying on various degrees on empiricism. In an extensive review of trailing-edge theories available at the time, Howe [4] identified three categories, (i) theories based on Lighthill's acoustic analogy, (ii) theories based on the solution of special problems approximated by linearized equations, and (iii) ad hoc models. Howe concluded that all methods, when interpreted properly, essentially gave similar results at vanishingly small Mach numbers. Trailing-edge noise experiments on a NACA-0012 airfoil by, for example, Brooks and Hodgson [5] supported the theoretical results.

The theory of Amiet [6], from category (ii), appears to be an attractive approach as the far-field noise can be predicted as a function of the surface pressure difference only, instead of having to provide the turbulence quadrupole sources in full. Amiet's classical trailing-edge theory considers the broadband noise generation of turbulent flow convecting past a semi-infinite flat plate at zero angle of attack. In most practical applications, airfoils have a finite thickness and be loaded to produce steady lift or thrust. Laboratory measurements made by Paterson and Amiet [7] for turbulent flow over a NACA-0012 airfoil showed that the flat-plate theory yields reasonable results for finite thickness airfoil geometries. However, it is not clear whether the noise radiation is unaffected by the airfoil geometry when looking at individual tonal components. For example, a theoretical study of leading-edge noise [8] found that the airfoil geometry in a cascade configuration had a significant effect on the tonal noise, while the broadband noise radiation is relatively unaffected due to cancelation effects when integrating over the entire spectrum.

Tonal noise from airfoil trailing edges can be a significant noise source [9,10] and has been linked in experiments [11,12] to an acoustic feedback mechanism involving boundary layer instabilities. This mechanism of tone noise generation was recently confirmed by direct numerical simulations (DNS) [13]. Another mechanism responsible for tonal noise from airfoils is the unsteady wake interacting with the trailing edge, which has been modeled by a reversed Sears' problem [14]. Furthermore, two-dimensional numerical

simulations of moderate Reynolds number flow over an airfoil with a rounded trailing edge [15] found that pressure fluctuations due to vortex shedding are substantial sources of sound. It can be argued that tonal noise generated by large scale vortices is a low Reynolds number phenomenon. However, Reynolds numbers for flow over airfoils of small wind turbines or small unmanned air vehicles can be sufficiently small to allow for laminar separation bubbles shedding vortices with a strong spanwise coherence on the suction side. Even for flows over airfoils at higher Reynolds number, Paterson et al. [9] found that fluctuations on the pressure side displayed a strong spanwise coherence. Therefore, the investigation of tonal noise from airfoils at moderate Reynolds numbers is of much practical interest as it is not clear whether the different noise components can be predicted using classical flat-plate theory, such as Amiet's trailing-edge noise theory.

The sustained growth in computing power over the years has made DNS of aerodynamically generated sound increasingly feasible. The advantage of directly solving the full unsteady Navier–Stokes equations is that both the near field hydrodynamics and the far-field sound can be obtained at the same time. Thus, DNS can be used to provide an insight into the physical mechanisms of sound generation and potentially help to validate acoustic theories. One of the key elements in Amiet's trailing-edge theory is the surface pressure jump function, required to determine the total surface pressure difference, and hence the equivalent dipole source strength over the airfoil surface. Experiments with turbulent flow over airfoils have suggested that the response function yields reasonable results for the radiated sound field [7,16]. However, the instrumentation of an airfoil with pressure sensors appears to only be possible up to a distance of roughly 1–2% of the chord-length from the trailing edge [16,17]. The behavior in the immediate vicinity of the trailing edge, in particular the surface pressure difference, can therefore not be investigated experimentally. In contrast, DNS provide surface pressure data over the entire surface, including the trailing edge itself. Sandberg et al. [18] conducted DNS of Tollmien–Schlichting (T–S) waves convecting over an infinitely thin flat plate with a trailing edge. They demonstrated that the surface pressure jump transfer function accurately predicts the DNS results over a range of Mach numbers and reduced frequencies. It was also shown that using this flat-plate theory allows the radiation to the far field to be predicted accurately, which was not obvious as full viscous DNS were compared with inviscid flat-plate theory.

The aim of the present paper is to extend this line of work and use DNS to research noise generated by flow over airfoils with different trailing-edge angles, and at various angles of attack. Of particular interest is the investigation of whether the approach of determining the far-field sound as a function of surface pressure difference yields satisfactory results for realistic airfoils at angles of attack, i.e. where the presence of a laminar separation bubble causes vortex shedding on the suction side. In addition, the performance of Amiet's surface pressure jump will be evaluated. DNS are conducted of NACA-0006, NACA-0008 and NACA-0012 airfoils at zero incidence. The trailing edge-angles for these airfoils are 8.4°, 11.2°, and 16.8°, respectively. Furthermore, DNS are performed of the NACA-0012 airfoil at two angles of attack. As in our previous study [18], to allow for parametric investigations, DNS are conducted in two dimensions. Because Amiet's classical theory considers three-dimensional sound radiation, a modification of Amiet's theory accounting for two-dimensional sound radiation [18] is employed. The results of the strictly two-dimensional theory are compared with the DNS data. For the present investigation, a high-order accurate numerical method is chosen which is free of upwinding, artificial dissipation or any form of explicit filtering.

2. Governing equations

The results from DNS will be compared to theoretical results derived using the two-dimensional flat-plate theory.

2.1. Direct numerical simulations

The flow under consideration is governed by the full compressible Navier–Stokes equations. The fluid is assumed to be an ideal gas with constant specific heat coefficients. All quantities are made dimensionless using the flow-quantities at a reference location in the flow; here the freestream/inflow location is used.

The non-dimensional continuity, momentum and the energy equations are

$$\frac{\partial \rho}{\partial t}+\frac{\partial}{\partial x_k}(\rho u_k)=0, \tag{1}$$

$$\frac{\partial}{\partial t}(\rho u_i)+\frac{\partial}{\partial x_k}[\rho u_i u_k+p\delta_{ik}-\tau_{ik}]=F_i, \tag{2}$$

$$\frac{\partial}{\partial t}(\rho E)+\frac{\partial}{\partial x_k}\left[\rho u_k\left(E+\frac{p}{\rho}\right)+q_k-u_i\tau_{ik}\right]=0, \tag{3}$$

where F_i is a volume force and the total energy is defined as $E=T/[\gamma(\gamma-1)M^2]+0.5u_iu_i$. The stress tensor and the heat-flux vector are computed as

$$\tau_{ik}=\frac{\mu}{Re}\left(\frac{\partial u_i}{\partial x_k}+\frac{\partial u_k}{\partial x_i}-\frac{2}{3}\frac{\partial u_j}{\partial x_j}\delta_{ik}\right), \quad q_k=\frac{-\mu}{(\gamma-1)M^2PrRe}\frac{\partial T}{\partial x_k}, \tag{4}$$

respectively, where the Prandtl number is assumed to be constant at $Pr=0.72$, and $\gamma=1.4$. The molecular viscosity μ is computed using Sutherland's law [19], setting the ratio of the Sutherland constant over freestream temperature to 0.368̀. To close the system of equations, the pressure is obtained from the non-dimensional equation of state $p=(\rho T)/(\gamma M^2)$. In order to introduce disturbances into the boundary layer on the suction side of the airfoil, a volume force F_i is added to the right-hand-side of the governing equations. To minimize the sound generation of the disturbances, a solenoidal and therefore quiet forcing is used [20].

2.2. Analytical solution

In the present investigation, two-dimensional laminar flows with single-frequency disturbances are investigated. A modification of Amiet's theory accounting for two-dimensional sound radiation of single-frequency disturbances was therefore previously derived [18]. Here, only the relevant results of the derivation are presented. The two-dimensional theory is applicable in the coordinate system $\mathbf{x}=[x_1,x_2]^{\mathrm{T}}$, where x_1 and x_2 are the streamwise and the wall normal directions, non-dimensionalized with the semi-chord b, respectively. A plate with zero thickness is assumed to be semi-infinite, i.e. the leading edge is not considered. However, the integration of the sources along the plate coordinate y_1 is conducted over the finite length $-2\leqslant y_1\leqslant 0$. The main modification to the original theory consists of replacing the three-dimensional Green's function with a two-dimensional Green's function to account for radiation in two dimensions only. Inserting the two-dimensional Green's function into Goldstein's formulation [21] of the acoustic analogy (neglecting viscosity and performing a Fourier transform in time) yields

$$p(\mathbf{x},\omega)=\frac{\mathrm{i}x_2\omega M}{4\beta}\int_{-2}^{0}\Delta p_t(\mathbf{y},\omega)\frac{1}{R}H_1^{(2)}\{\mu_0[M(y_1-x_1)+R]\}\,\mathrm{d}y_1, \tag{5}$$

where ω is the frequency, $\beta=\sqrt{(1-M^2)}$, $R=\sqrt{(y_1-x_1)^2+\beta^2(y_2-x_2)^2}$, and c represents the speed of sound. The reduced frequency is $\mu_0=\omega b/(c\beta^2)$ and $H_1^{(2)}$ denotes a first-order Hankel function of the second kind. The total pressure fluctuations on each surface consist of the sum of the incident pressure, p_i, and the scattered pressure, p_s. For the case of pressure disturbances being generated on the top side of the airfoil, the total pressure on that surface is $p_{t_{\mathrm{top}}}=p_i+p_s$ [6]. On the bottom side, in the absence of an incident pressure disturbance, $p_{t_{\mathrm{bot}}}=-p_s$ [6]. From these two relations, the total surface pressure difference can be evaluated as

$$\Delta p_t=p_{t_{\mathrm{top}}}-p_{t_{\mathrm{bot}}}=\Delta p_i+\Delta p_s, \tag{6}$$

with $\Delta p_i=p_{i_{\mathrm{top}}}-p_{i_{\mathrm{bot}}}$ and $\Delta p_s=p_{s_{\mathrm{top}}}-p_{s_{\mathrm{bot}}}$. Since the scattered pressure field on the top and bottom sides of the trailing edge are equal in magnitude but opposite in sign, i.e. in anti-phase, the incident pressure field can be computed from the total surface pressures according to

$$p_i=p_{t_{\mathrm{top}}}+p_{t_{\mathrm{bot}}}. \tag{7}$$

In cases where the entire time-series of the surface pressures is available (which it is for DNS) Eq. (5) can be integrated directly to obtain the acoustic pressure field. This method is denoted as *using the acoustic analogy* in the following. However, when only the incident pressure field is known, the total pressure field at the trailing edge can be determined from the incident pressure field through a transfer function [22]. As a prerequisite, the unsteady Kutta condition is assumed to hold at the trailing edge, i.e. $\Delta p_t = 0$, and the condition of no-flow across the plate is imposed. With the above conditions, the Schwarzschild solution can be employed to derive a surface pressure jump function H_S [22] (for incident pressure fluctuations on one side of the airfoil), defined by

$$\Delta p_s(y_1, K_x) = H_S(y_1, K_x) p_i(y_1, K_x)$$

with

$$H_S(y_1, K_x) = \{(1+\mathrm{i})E^*[-(\mu_0(1+M)+K_x)y_1] - 1\}. \tag{8}$$

The function E^* is a combination of Fresnel integrals. Therefore, the total pressure difference becomes

$$\Delta p_t(y_1, K_x) = H_D(y_1, K_x) p_i(y_1, K_x) = [f_i(y_1, K_x) + H_S(y_1, K_x)] p_i(y_1, K_x). \tag{9}$$

In Amiet's original paper [6] $f_i(y_1, K_x)$ was set to unity to account for the incident pressure. However, a convergence factor ε was subsequently introduced [23] to gradually decrease the incident pressure towards the leading edge such that $f_i(y_1, K_x) = \exp(\varepsilon K_x y_1)$. To account for back-scattering from the leading edge, Roger and Moreau [24,25] derived an extension to Amiet's original equation. However, the leading-edge correction is not considered in the current work as it was shown to have only a small effect on the far-field noise for non-dimensional frequencies exceeding '$kb = 10$', corresponding to $\mu_0 \gtrsim 3$.

Inserting Eq. (9) into Eq. (5) yields the two-dimensional acoustic pressure field as a function of the incident pressure field

$$p(\mathbf{x}, \omega) = \frac{\mathrm{i}x_2 \omega M}{4\beta} \int_{-2}^{0} H_D(y_1, K_x) p_i(y_1, K_x) \frac{1}{R} H_1^{(2)}\{\mu_0[M(y_1 - x_1) + R]\}\, \mathrm{d}y_1. \tag{10}$$

Note that, in contrast to the original theory, no far-field approximation has been made. In the following, computing the acoustic pressure with Eq. (10) is denoted as *using the modified theory of Amiet*.

3. Numerical method

The compressible Navier–Stokes equations are solved using a high-order numerical scheme applicable to general geometries. The extension to general coordinates is achieved through metric terms pre-multiplying the derivatives of the governing equations. No upwinding, artificial dissipation or explicit filtering is employed. Stability is achieved through appropriate conditioning of the governing equations, including splitting the nonlinear terms into conservative and non-conservative parts and a Laplacian formulation of the viscous and heat conduction terms. The latter is used to avoid odd–even decoupling when using central finite-difference schemes. In addition, compatible spatial difference operators for the interior and boundary points are employed. Further details on the fundamental numerical approach are given in Sandham et al. [26]. A non-reflecting zonal boundary condition is used to avoid spurious pressure-oscillations from the boundaries, in particular the outflow boundary which is subject to the passage of vortical structures. The method is based on commonly used characteristic boundary conditions. Here, incoming characteristics are ramped to zero in a buffer zone as opposed to merely setting them to zero at the boundary [27]. Crucially, in contrast to most other zonal approaches, the method is free of coefficients that require calibration and only the length of the fringe zone needs to be specified.

For the analytical approach, Eq. (5) or (10) are integrated using a fourth-order accurate scheme. The plate is discretized with a non-uniform grid, clustering most points in the vicinity of the trailing edge to reduce computational cost. A thorough validation of both numerical codes was presented previously [18]. The numerical treatment of the trailing edge for the airfoil simulations is the same as in the previous flat-plate simulations [18], and is therefore considered a reliable representation of the geometric singularity.

4. Results

DNS of compressible flow over symmetric NACA airfoils were conducted at $\alpha = 0^\circ$, 5°, and 7° at $M = 0.4$. The Mach number was chosen as a compromise between a large enough Mach number to allow for a feasible time-step in the compressible Navier–Stokes code, and a Mach number sufficiently small to avoid local supersonic flow for the airfoils at high incidence. The Reynolds number based on chord and the freestream velocity was specified as $Re = 5 \times 10^4$. For all cases, the computational domain has the dimensions $-12.6 \leqslant x_1 \leqslant 14$ and $-14.6 \leqslant x_2 \leqslant 14.6$, with the trailing edge located at $x_1 = x_2 = 0$. The numerical grids were designed using an iterative method [28]. At zero incidence, the domain is discretized using 2243 and 692 non-equidistantly spaced points in the tangential and normal directions with respect to the airfoil surface. At $\alpha = 5^\circ$ and 7° the domain is discretized with 2570×692 and 2587×692 points, respectively, where the additional tangential points are added to the suction side of the airfoil. The simulations were conducted until the initial transients had left the computational domain and quasi-time-periodic states were reached. For the zero incidence cases, forcing was applied to the upper surface, located at $y_1 = -1.8$, to excite T–S waves. The forcing frequency was chosen as the most unstable frequency obtained from linear stability simulations of the respective mean flow, i.e. $\mu_0 = 4.8$, 7.04, and 8.33 for the NACA-0006, NACA-0008, and NACA-0012 cases, respectively. The amplitude of the volume forcing was selected such that the amplitude of the surface pressure difference at the streamwise position of the forcing was approximately 5×10^{-4}. This amplitude was chosen to avoid nonlinear saturation levels of the T–S waves that would have resulted in the generation of higher harmonics. On the other hand, the amplitude needed to exceed a lower threshold so that the sound field

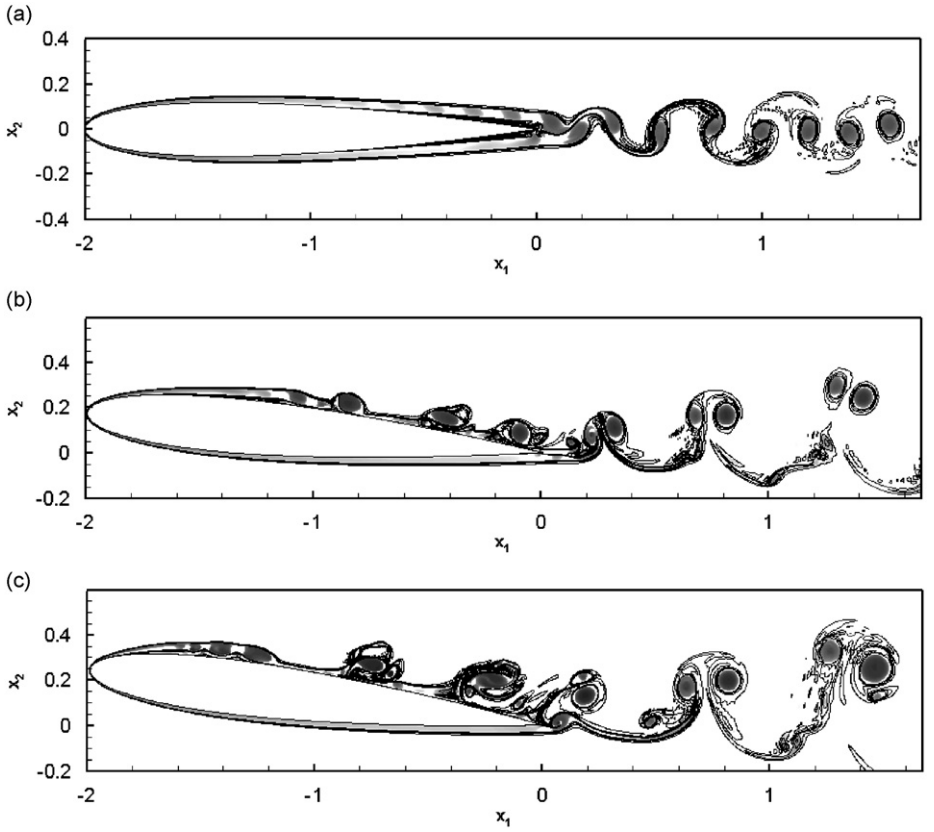

Fig. 1. Instantaneous contour lines of the spanwise vorticity component, eight levels in range $[-20; 20]$; and contours of the second invariant of the velocity-gradient tensor, 20 logarithmically spaced levels in range $[1, 1 \times 10^4]$, for NACA-0012 at $\alpha = 0^\circ$ (a), $\alpha = 5^\circ$ (b), and $\alpha = 7^\circ$ (c).

could be reliably detected at a distance from the trailing edge. The objective was to generate an incident pressure
field so that the evaluation of Amiet's surface pressure jump function could be accomplished. Without the forcing the zero incidence airfoil is subject only to the induced pressure fluctuations by the unsteady wake.

Instantaneous contour lines of the spanwise vorticity component and contours of the second invariant of the velocity-gradient tensor are shown in Fig. 1 to give an impression of the flow fields around the NACA-00012 airfoil at three different angles of attack. At zero incidence, the flow is symmetric on the top and bottom sides, except for the (T–S) waves that are only introduced on the top side. However, their amplitude is sufficiently small not to affect the mean flow and the waves are only visible due to the logarithmic scale chosen for the second invariant of the velocity-gradient tensor. An unsteady wake develops downstream of the trailing edge. For the airfoils at non-zero angles of attack, explicit forcing was not required, as a laminar separation bubble was present and vortex shedding occurred on the suction side of the surface, as shown in Figs. 1(b) and (c). These vortices produce pressure disturbances that convect over the surface of the airfoil and pass over the trailing edge. The main difference between the two airfoils at an angle of attack is that for the $\alpha = 7^\circ$ case the separation bubble, and the first occurrence of vortex shedding, is located considerably farther upstream compared with the $\alpha = 5^\circ$ case. In addition, the flow field appears to be more complex at higher incidence, in particular in the vicinity of the trailing edge.

The main objective of this paper is to investigate the trailing-edge noise generation. It is therefore essential that noise generated by the airfoil is represented accurately by the simulations and that reflections from boundaries do not interfere with the airfoil self-noise. In Fig. 2 instantaneous contours of dilatation rates are shown for the NACA-0012 airfoil. For all angles of attack, sound waves can clearly be seen originating from the airfoil. The zonal characteristic boundary condition is able to sufficiently reduce reflections caused by the wake structures passing the outflow boundary. For both zero incidence and $\alpha = 5^\circ$ it appears as if the sound field consists of a single tone radiating from the trailing edge. At $\alpha = 7^\circ$ the nature of the dilatation field changes. On the bottom side of the airfoil the sound waves originate from the trailing edge. On the top side, however, additional sources are present, generating a considerably more complex sound field.

With more than one frequency present in the acoustic field it is necessary to Fourier transform the DNS data with respect to time to investigate the trailing-edge noise in frequency space. To obtain smoother spectra, Hanning windowing and averaging over multiple segments with a 50% overlap is employed [29]. The power spectrum S_p is then computed by multiplying the point spectrum with its complex conjugate, dividing by the record length, and applying the factor $\frac{8}{3}$ to account for the spectral window.

Fig. 3 shows power spectra of the surface pressure difference at the trailing edge compared with spectra from pressure probes located above, $\mathbf{x} = (-1, 1.2)$, and below, $\mathbf{x} = (-1, -1.2)$, the airfoil for all cases conducted of the NACA-0012 airfoil. Note that the amplitudes of the spectra obtained in the acoustic field are scaled with arbitrary constants to allow for clearer comparison. In the zero incidence case (Fig. 3(a)) two distinct peaks can be observed in the surface pressure difference spectrum, one at the frequency of the unsteady wake, $\mu_0 = 6.58$, and one at the forcing frequency of the T–S wave, $\mu_0 = 8.33$. The fluctuations at the trailing edge due to the wake occur at a considerably higher amplitude than those caused by the passing of the T–S wave. In Amiet's classical trailing-edge theory which is concerned with turbulent flow, the converse is true. The fluctuations convecting over the surface will be larger than the wake induced fluctuations. Scrutinizing the pressure spectra at positions above and below the airfoil, the pressure at the wake frequency exhibits a much larger amplitude than at the T–S frequency. This explains why the sound field appeared to consist only of a single tone in Fig. 2. Nevertheless, both frequencies are present and will be investigated individually in the following section.

At $\alpha = 5^\circ$ (Fig. 3(b)), the pronounced peak at $\mu_0 = 5.05$ is associated with the vortex shedding on the suction side of the airfoil. Higher harmonics of the shedding frequency also appear in the spectrum at fairly high amplitude. The spectra of the acoustic field above and below the airfoil again only show a single pronounced peak, at the fundamental frequency of the vortex shedding. For the highest angle of attack investigated the spectrum is fundamentally different, displaying a more broadband-like behavior than the distinct peaks associated with tones for the lower angles of attack. A peak in the spectrum occurs at $\mu_0 = 3.71$.

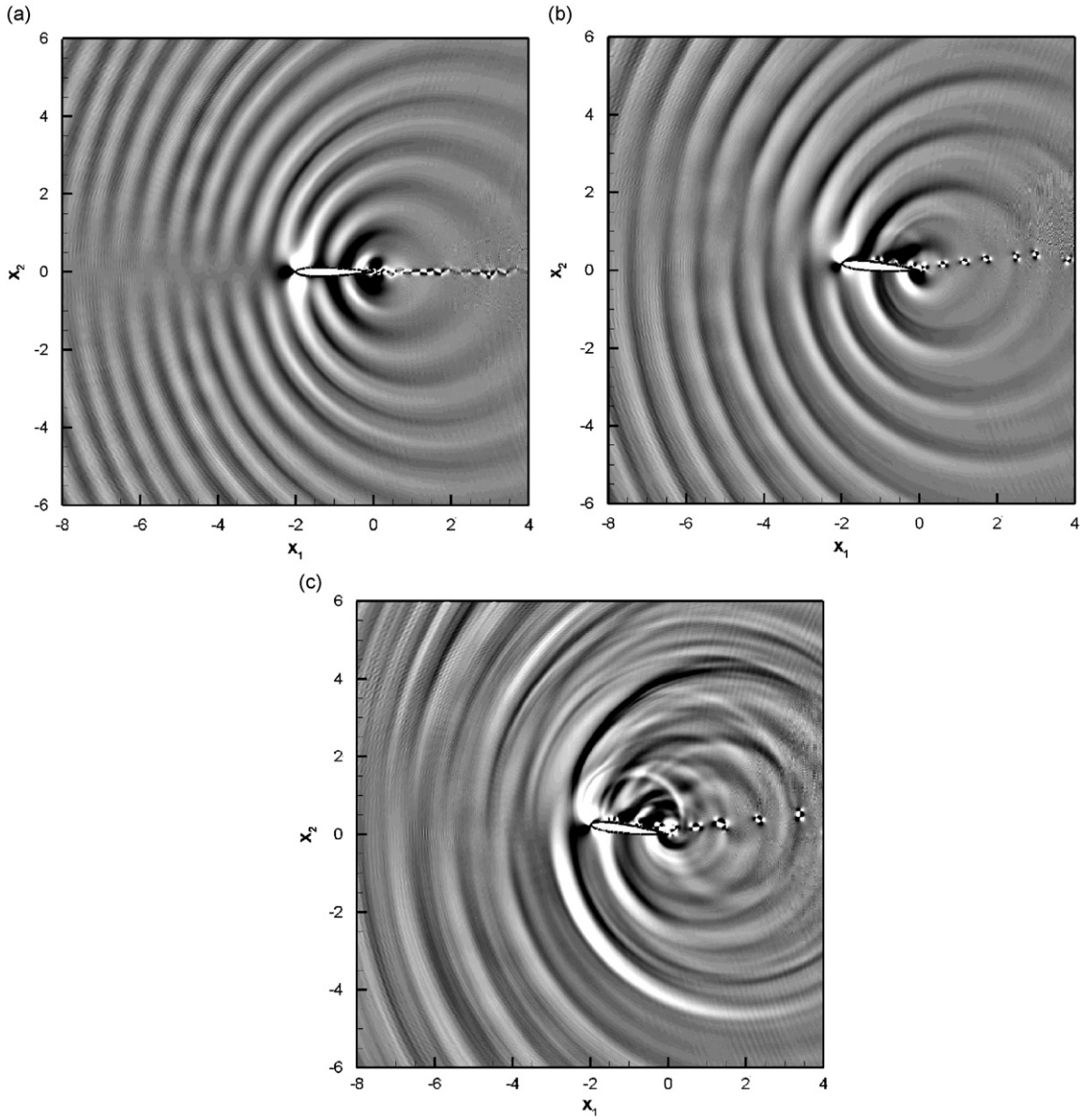

Fig. 2. Instantaneous contours of dilatation for NACA-0012 at $\alpha = 0^\circ$ (a), $\alpha = 5^\circ$ (b), and $\alpha = 7^\circ$ (c), 20 levels in range $[-0.05; 0.05]$ for (a), otherwise $[-0.1; 0.1]$.

In contrast to the smaller incidence cases, the spectra from the pressure probes above and below the airfoil display very different amplitudes. In particular at higher frequencies, the pressure amplitudes above the airfoil are considerably larger than on the bottom side. The intuitive explanation for this observation is that the additional sources visible in Fig. 2 only radiate from the top side of the airfoil. Therefore, above the airfoil the trailing-edge noise will be superposed with the noise from the additional sources while on the lower side the pressure sensor will detect trailing edge only. Overall, the simulations can be divided into two distinct categories. At zero incidence the sound waves appear to be generated by the unsteadiness of the wake, whereas for higher angles of attack the noise is generated predominantly by coherent vortices being shed on the suction side of the airfoil and passing over the trailing edge. In the following, the accuracy of Amiet's surface pressure jump function and the prediction of the acoustic pressure based on the surface pressure difference will be investigated for each angle of attack individually.

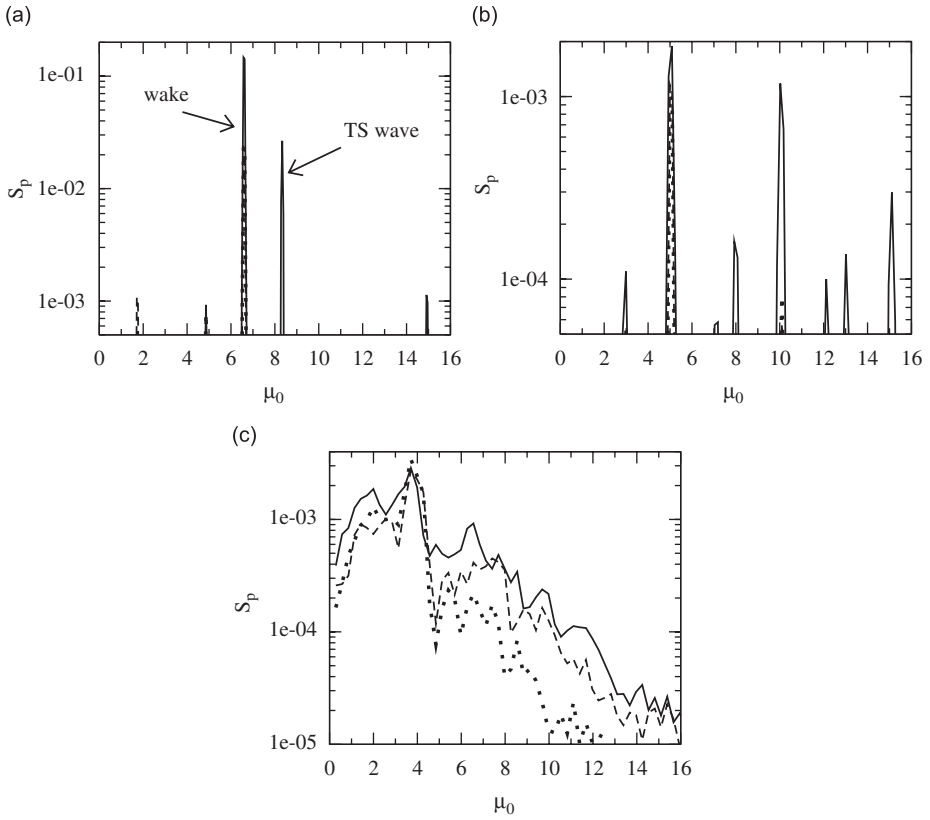

Fig. 3. Power spectra of (—) surface pressure difference Δp_t at the trailing edge, (– – –) pressure on top side of airfoil, (· · ·) pressure on bottom side of airfoil; amplitudes of acoustic pressure on top and bottom side multiplied by a; $\alpha = 0^\circ$, $a = 1000$ (a), $\alpha = 5^\circ$, $a = 10$ (b), and $\alpha = 7^\circ$, $a = 100$ (c).

4.1. *Airfoil at* $\alpha = 0^\circ$

The sound radiated by the airfoil at zero incidence contains two distinct frequencies, the wake shedding frequency and the T–S wave frequency. For the wake frequency, no incident pressure field is present, implying that the pressure disturbances recorded on the surface are induced by the unsteady wake downstream of the trailing edge. From Fig. 2(a) it is evident that the sound radiated to the far field is of opposite phase on the top and bottom side of the airfoil, a characteristic of the scattered pressure field, as discussed in Section 2.2.

Because the total surface pressure fluctuation contains only the contribution from the scattered pressure field for this particular case of $\alpha = 0^\circ$, according to Eq. (6) the total pressure difference can be evaluated from $\Delta p_t = 2p_s = 2p_{t_{\text{top}}} = 2p_{t_{\text{bot}}}$. Each grid point of the top and bottom surfaces of the airfoil was projected onto the chord line in order to evaluate the surface pressure difference Δp_t for each y_1 position. The real part of the total pressure for both the top and bottom surface is shown in Fig. 4(a). The key observation is that the amplitude of the pressure fluctuations increases up to a location very close to the trailing edge ($y_1 \approx -0.012$) before decaying slightly towards the trailing edge. The location of the peak of the pressure fluctuation is governed by the Reynolds number and can be predicted by triple-deck-theory. Sandberg and Sandham [30] conducted a DNS of flow past a flat-plate trailing edge with a similar grid resolution of the trailing-edge region, and found that the inner solution of the triple-deck-theory was resolved. The pressure field across the trailing edge was continuous, although the significant gradient from the trailing-edge point to the first point downstream of the trailing edge caused slight numerical oscillations, as seen when looking very closely at Fig. 4(a). For that reason, a resolution study of the trailing-edge region was conducted which found that the oscillations were reduced and the amplitude of the pressure fluctuation peak remained finite.

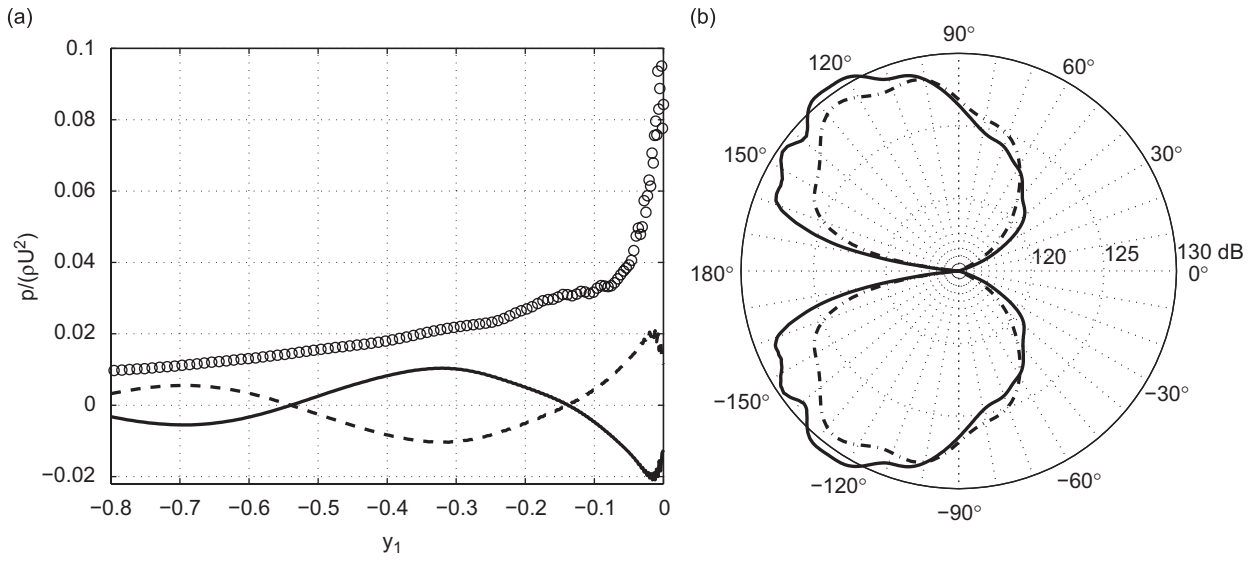

Fig. 4. Surface pressure (a); (—) real part of p_{top}, (− − −) real part of p_{bot}, (○) magnitude of Δp_t; magnitude of acoustic pressure at $R_d = 4$ (b); (− · −) using the acoustic analogy with $\Delta p_t = p_{t_{\text{top}}} - p_{t_{\text{bot}}}$, (—) acoustic pressure from DNS; $\mu_0 = 6.58$, $\alpha = 0^\circ$.

However, qualitatively, the pressure field remained the same, thus implying that the numerical treatment of the geometrical singularity was adequate.

Because the pressure at the top and bottom side is 180° out of phase, the surface pressure difference is twice the amplitude of either the top or bottom side, resulting in a large value of Δp_t at the trailing edge, as illustrated by the open circles denoting the magnitude of surface pressure difference. This is clearly inconsistent with the unsteady Kutta condition, which requires $\Delta p_t = 0$ at the trailing edge. For a blunt trailing edge, Roger et al. [14] argued that vortex shedding induces pressure fluctuations on both sides of the surface which are in phase opposition, and hence the Kutta condition fails if the plate is modeled to be infinitely thin. The current results show that this also applies to an airfoil with a sharp trailing edge where vortex shedding occurs at a distance downstream of the trailing edge. We now investigate whether the acoustic pressure can be predicted accurately as a function of the surface pressure difference using the theory due to Amiet for a flat plate. The results obtained using the acoustic analogy with $\Delta p_t = p_{t_{\text{top}}} - p_{t_{\text{bot}}}$ are compared with the acoustic pressure computed directly with DNS in Fig. 4(b). The directivity is predicted correctly and the amplitude lies within 2 dB, except at $\theta \approx \pm 150^\circ$ where a difference in amplitude of roughly 5 dB can be observed. Overall the agreement between the predicted values and the DNS data is good, considering that the geometry of this relatively thick airfoil is not accounted for and the inviscid theory is compared with data from a viscous simulation. The fact that the acoustic pressure can be predicted reasonably well based on the surface pressure difference implies that the main source of sound is the induced pressure difference on the airfoil surface and not the vortex shedding in the wake itself, as suggested previously for an airfoil with a rounded trailing edge [15].

At the forced frequency $\mu_0 = 8.33$, incident pressure waves are present in the form of T–S waves, and the surface pressure jump function can therefore be tested. The incident pressure is computed using Eq. (7) and the total surface pressure difference is then evaluated from Eq. (9). The convection speed of the instability wave, an input parameter that enters the surface pressure jump function through the non-dimensional wavenumber K_x, is determined from the DNS data to be $U_c = 0.52$. The predicted surface pressure difference is compared to $\Delta p_t = p_{t_{\text{top}}} - p_{t_{\text{bot}}}$ in Fig. 5(a). The magnitude of the surface pressure difference obtained directly from DNS increases considerably over the chord, reaching its maximum value at the trailing edge. Amiet's surface pressure jump function assumes the unsteady Kutta condition to hold, thus the predicted Δp_t is zero at the trailing edge. Moreover, the 'phase' of the surface pressure difference computed using the surface pressure jump function does not agree with the DNS data. To account for the difference in phase observed in Fig. 5(a), the total pressure difference was evaluated by subtracting the scattered pressure from the incidence pressure

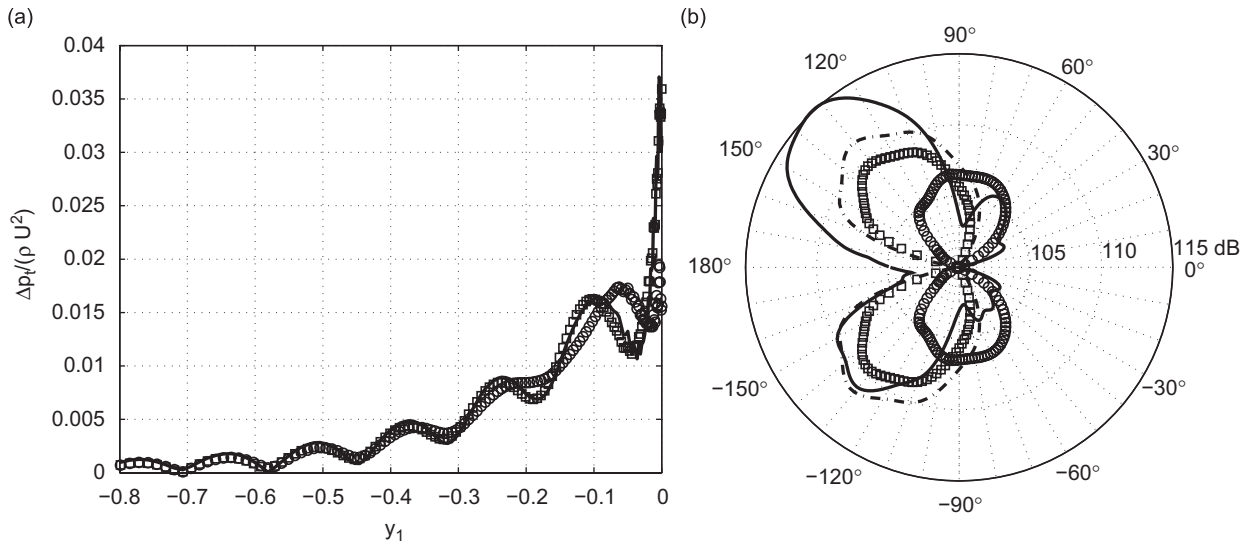

Fig. 5. Magnitude of total surface pressure difference (a) and magnitude of acoustic pressure at $R_d = 2$ (b); $(- \cdot -)$ $\Delta p_t = p_{t_{\text{top}}} - p_{t_{\text{bot}}}$, $(\circ)$ $\Delta p_t = (1 + H_S)p_i$, $(\square)$ $\Delta p_t = (1 - H_S)p_i$, (—) acoustic pressure from DNS; $U_c = 0.52$, $\mu_0 = 8.33$, $\alpha = 0^\circ$.

according to $\Delta p_t = (1 - H_S)p_i$, i.e. with the sign of H_S reversed. This profound modification results in an entirely different behavior of the surface pressure difference, which now agrees well with the DNS data. Instead of obtaining a zero pressure difference at the trailing edge, this modification results in a doubling of the incident pressure field at the trailing edge. This observation was unforseen and is contrary to the results obtained in our previous simulations of flat-plate trailing edges [18]. To exclude the possibility that this unexpected phenomenon is due to the numerical procedure of the simulation, an additional DNS was performed using a different numerical treatment of the trailing edge which yielded the same result. The good agreement between the predicted surface pressure difference and the DNS data implies that Amiet's surface pressure jump function H_S accurately predicts the scattered pressure, albeit with a sign change that is discussed further in the next section. Therefore, in spite of being derived for a flat plate, it appears to be applicable to an airfoil with finite thickness.

When using the acoustic analogy to predict the acoustic pressure at the T–S frequency $\mu_0 = 8.33$, the directivity found with DNS is captured (see Fig. 5(b)). However, the amplitude is predicted fairly accurately for the lower side only, which should be due to noise radiation of the scattered pressure field. Above the airfoil, the DNS data show amplitudes of up to 5 dB larger than on the lower side. The acoustic analogy is based on the surface pressure difference and will therefore predict a symmetric pattern with respect to $x_2 = 0$. Employing the modified theory of Amiet using Eq. (9) to compute the surface pressure difference, the agreement with the DNS data is poor. This was expected, as an accurate representation of the source terms on the surface is a prerequisite for accurately predicting the acoustic field, which is not seen in Fig. 5(a). When accounting for the unexpected phase shift by reversing the sign of H_S, as discussed above, the prediction of the far-field sound is similar to that obtained using the acoustic analogy.

It is also noteworthy that additional downstream pointing lobes are visible in the DNS data which are not predicted by the acoustic analogy. These additional lobes might be an indication for the existence of an additional noise source due to the nonlinear interaction between the T–S wave and the instability wave of the wake, as previously seen for flat-plate trailing-edge simulations [18].

4.2. *Effect of thickness for airfoil at* $\alpha = 0^\circ$

The fundamental difference between the current airfoil simulation and the flat-plate results is the finite thickness of the airfoil. Therefore, in an attempt to elucidate the exact mechanism for the unforeseen change in

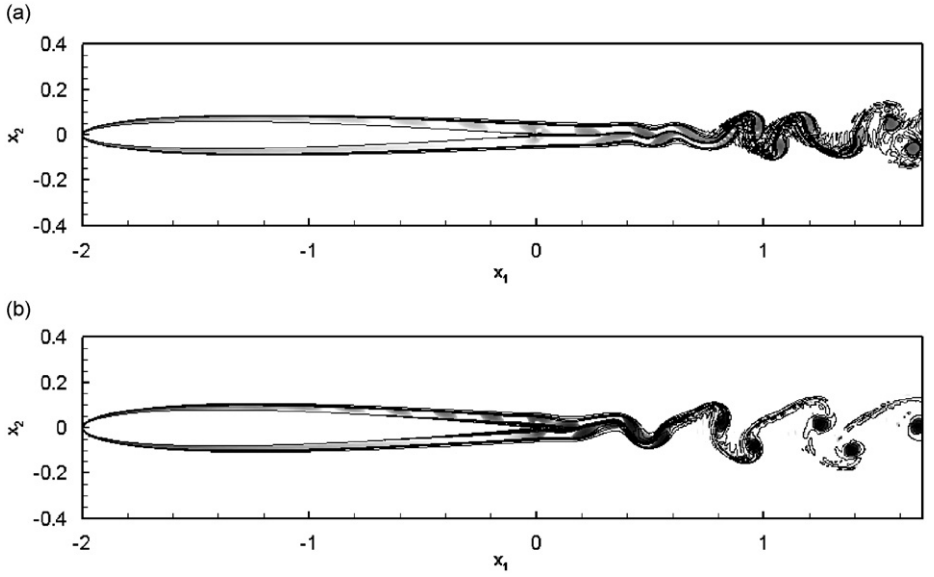

Fig. 6. Instantaneous contour lines of the spanwise vorticity component, eight levels in range $[-20; 20]$; and contours of the second invariant of the velocity-gradient tensor, 20 logarithmically spaced levels in range $[1, 1 \times 10^4]$, for NACA-0006 (a), and NACA-0008 (b); $\alpha = 0^\circ$.

phase discussed above, additional DNS were conducted of NACA-0006 and NACA-0008 airfoils, which have smaller trailing-edge angles, to investigate the effect of the thickness on the surface pressure difference. The hydrodynamic field of the thinner airfoils is visualized using instantaneous contour lines of the spanwise vorticity component and contours of the second invariant of the velocity-gradient tensor, shown in Fig. 6. Both cases appear similar to the NACA-0012 case at zero incidence (Fig. 1(a)), i.e. the flow is symmetric on the top and bottom sides, except for the growing T–S waves present on the suction side. However, the thinner the airfoil the farther downstream the unsteady shedding in the wake occurs.

The power spectra of the two thinner airfoils at zero incidence are shown in Fig. 7. A distinct peak can be observed in the surface pressure difference spectrum at the frequency of the forcing for both cases. However, the other peak represents a higher harmonic of the fundamental frequency rather than a separate frequency of the wake. In the spectra of the pressure at positions above and below the airfoil, only the forcing frequency has a significant amplitude. The fact that only the forcing frequency is dominant in the spectra, as opposed to both the forcing frequency and a different wake frequency being present in the NACA-0012 case, implies that the wake unsteadiness locks into the forcing frequency.

The validity of the surface pressure jump function is tested for the thinner airfoils by evaluating the incident pressure with Eq. (7) and then computing the total surface pressure difference using Eq. (9), specifying $U_c = 0.45$ and $U_c = 0.48$ for the NACA-0006 and NACA-0008 cases, respectively. The predicted surface pressure difference is compared to $\Delta p_t = p_{t_{\text{top}}} - p_{t_{\text{bot}}}$ in Fig. 8(a) for the NACA-0006 case only, as the results for the NACA-0008 case are similar. As for the thicker airfoil, the magnitude of the surface pressure difference obtained directly from DNS increases considerably over the chord, indicating that the instability wave is strongly amplified. However, in contrast to the NACA-0012 case, Δp_t decays to zero at the trailing edge, thus satisfying the Kutta condition. Computing the surface pressure difference using the original formulation (9), i.e. without the phase change between the incident and scattered pressure required for the NACA-0012 case, the result agrees surprisingly well with the DNS data. This result confirms that Amiet's surface pressure jump function H_S can accurately predict the scattered pressure field for thin airfoils.

The directivity predicted using the acoustic analogy compares significantly better with the DNS data than in the NACA-0012 case, deviating less than 2 dB for all angles, as shown in Fig. 8(b). This can be attributed to the airfoil being considerably thinner, making the flat-plate assumption more accurate. Because the prediction

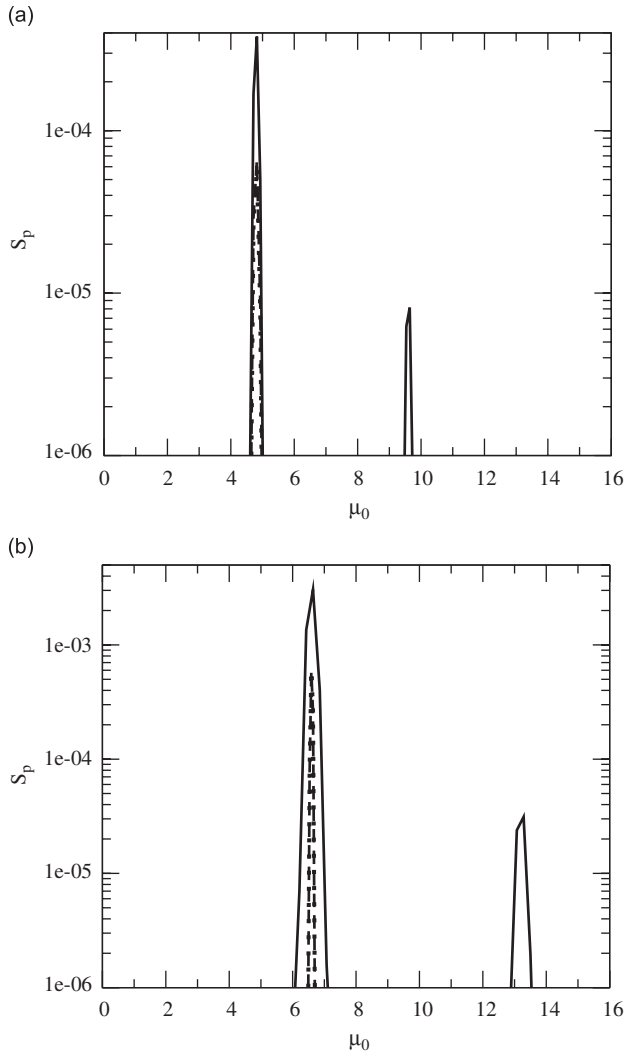

Fig. 7. Power spectra of (—) surface pressure difference Δp_t at the trailing edge, (– – –) pressure on top side of airfoil, (···) pressure on bottom side of airfoil; amplitudes of acoustic pressure on top and bottom side multiplied by a; NACA-0006, $a = 1000$ (a), NACA-0008, $a = 100$ (b); $\alpha = 0^\circ$.

of the total surface pressure difference is accurate, the directivity obtained from the modified theory of Amiet using Eq. (9) is accurate, albeit the amplitude is underpredicted by several dB. Another striking observation is that the additional downstream-pointing lobes that were present in the NACA-0012 case are not present for either NACA-0006 or NACA-0008 airfoils. This was expected as the wake frequency has locked into the frequency and the interaction between the two distinct frequencies cannot occur.

At the present time it remains unclear why the wake frequency locks into the forcing frequency for the thin airfoils, while it does not for the NACA-0012 airfoil. A possible reason can be deduced by scrutinizing the time-averaged streamwise velocity component U along the $x_2 = 0$ line, shown in Fig. 9. In the NACA-0012 case, after an initial peak, U becomes negative before increasing to positive values farther downstream, i.e. a reverse flow region is present. This reverse flow region is caused by flow oscillating around the trailing-edge corner at the wake frequency. The oncoming T–S waves therefore are subject to flow at the trailing edge alternating its direction at a different frequency. This might be responsible for the phase shift between the incident and scattered pressure fields. For the thin NACA-0006 and NACA-0008 airfoils, the streamwise

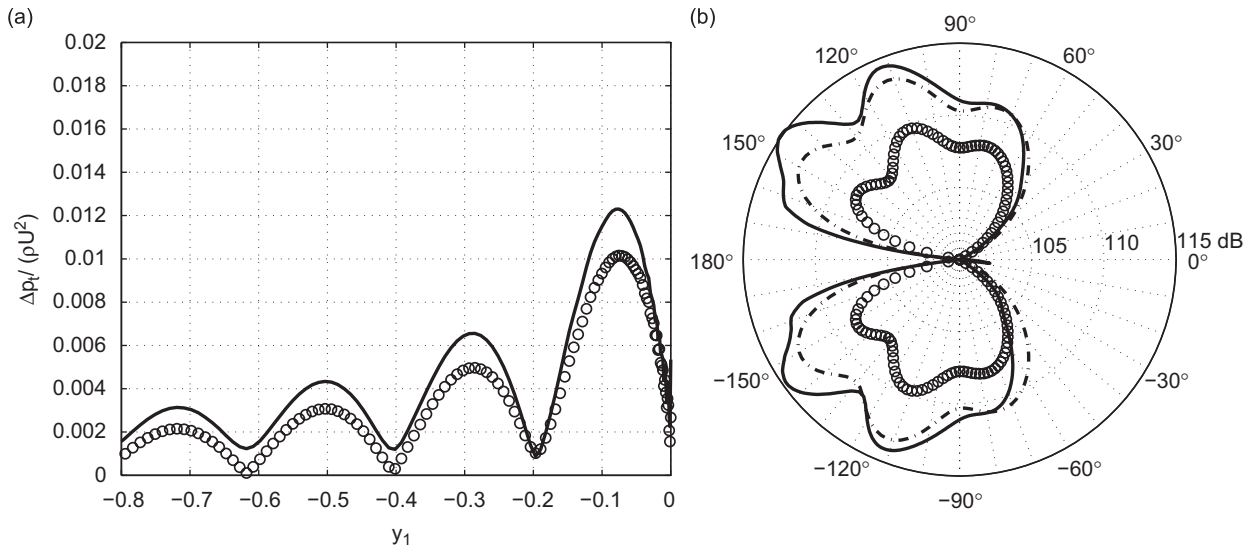

Fig. 8. Magnitude of total surface pressure difference (a), and magnitude of acoustic pressure at $R_d = 4$ for (b) NACA-0006; (– · –) $\Delta p_t = p_{t_{\text{top}}} - p_{t_{\text{bot}}}$, (○) $\Delta p_t = (1 + H_S)p_i$, (—) acoustic pressure from DNS; $U_c = 0.48$, $\mu_0 = 4.8$, $\alpha = 0^\circ$.

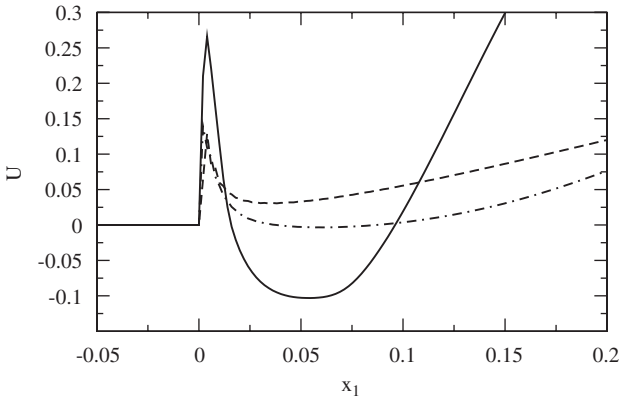

Fig. 9. Time averaged streamwise velocity component on $x_2 = 0$; (- - -) NACA-0006, (– · –) NACA-0008, (—) NACA-0012; $\alpha = 0^\circ$.

velocity component is positive along the entire x_1-axis, hence no reverse flow is present. In that case the flow leaves the airfoil tangentially, satisfying the Kutta condition as shown in Fig. 8, and a regular scattering process occurs. The fact that U is very close to becoming negative in the NACA-0008 case suggests that a further increase in airfoil thickness beyond 8% chord, i.e. an increase of the trailing-edge angle beyond 11.2°, will lead to the change of phase between incident and scattered pressure fields observed in the NACA-0012 case at the T–S frequency.

4.3. *Airfoil at* $\alpha = 5^\circ$

When the airfoil is set to a positive angle of attack, a fundamentally different flow pattern develops, as was shown in Figs. 1(b) and (c). A laminar separation bubble is present and vortices are shed on the suction side of the airfoil and then convect past the trailing edge.

With pressure disturbances caused by the vortex shedding convecting over the trailing edge the accuracy of the surface pressure jump function can again be evaluated. As previously described, the total surface pressure difference is evaluated from Eq. (9) with the incident pressure field determined from Eq. (7). The convection

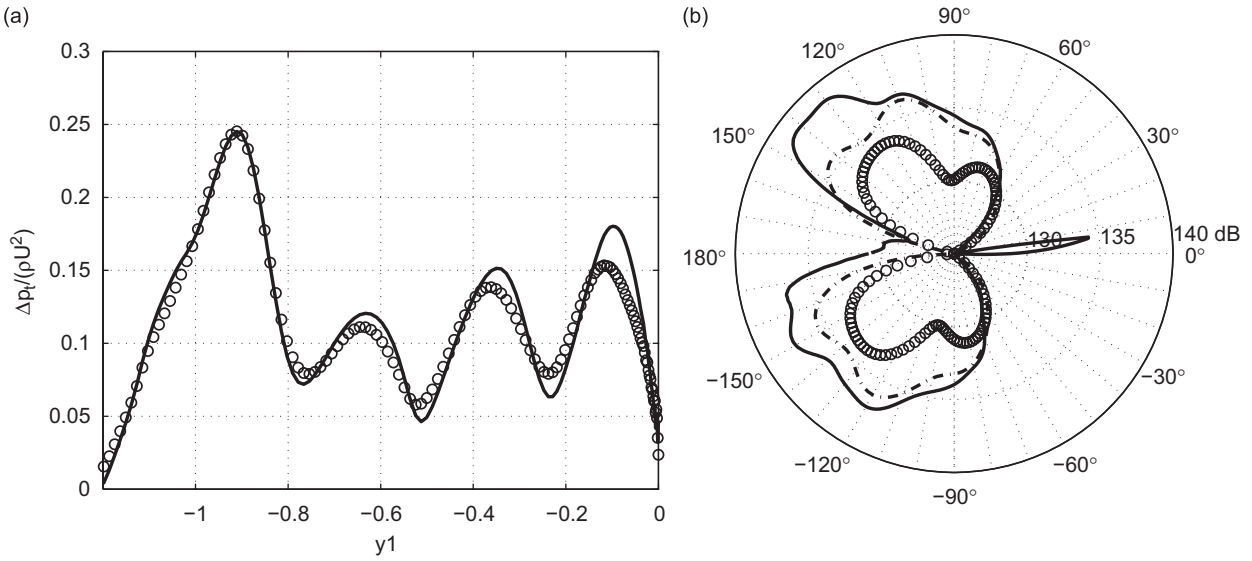

Fig. 10. Magnitude of total surface pressure difference (a), and magnitude of acoustic pressure at $R_d = 4$ (b); $(- \cdot -)$ $\Delta p_t = p_{\text{top}} - p_{\text{bot}}$, $(\circ)$ $\Delta p_t = (1 + H_S)p_i$, (—) acoustic pressure from DNS; $U_c = 0.62$, $\mu_0 = 5.05$, $\alpha = 5^\circ$.

speed of the vortical structures close to the trailing edge is determined as $U_c = 0.62$. Fig. 10(a) shows the magnitude of the computed total surface pressure difference compared with the DNS data. A pressure peak is evident at the shedding location, followed by several additional peaks growing in amplitude in the downstream direction. In contrast to the zero incidence case for a NACA-0012 airfoil, the amplitude of the surface pressure difference decreases significantly towards the trailing edge, suggesting that the Kutta condition is a reasonable assumption for this case. Naturally, the predicted Δp_t shows the same behavior close to the trailing edge, as the Kutta condition is imposed through the response function. In general, the predicted surface pressure difference agrees reasonably well with the DNS data, except for an error in the amplitude, implying that the surface pressure jump function also produces fairly accurate results at small angles of attack.

The directivity predicted with the acoustic analogy and the modified theory of Amiet are compared to the DNS data in Fig. 10(b). The directivity obtained from DNS shows a nearly symmetric distribution above and below the airfoil, indicating that the noise is mainly generated at the trailing edge. The directivity distribution from the acoustic analogy, which uses the surface pressure difference obtained from DNS, agrees closely with the DNS data. However, the amplitude is underpredicted by approximately 2 dB for angles up to $\theta = \pm 110^\circ$, and even larger differences in amplitude are present for larger angles, i.e. in the upstream direction. Nevertheless, the agreement between the predicted values and the DNS data is reasonable, considering that the geometry of the airfoil, the angle of attack and viscous effects is not taken into account by the flat-plate theory. When using the modified theory of Amiet, the directivity is well predicted, but the amplitude level is significantly lower than that obtained from the DNS data. This is a direct consequence of the lower amplitude obtained for the surface pressure difference computed using Amiet's response function.

4.4. *Airfoil at* $\alpha = 7^\circ$

When the angle of attack is increased further the hydrodynamic and acoustic fields become considerably more complex (see Figs. 1 and 2, respectively). At $\alpha = 7^\circ$ the pressure radiation spectrum displays a more broadband behavior than the other cases. Therefore, in the following, three different frequencies have been selected to establish whether frequency dependent phenomena occur: (i) $\mu_0 = 2.0$ where the acoustic wave length is on the order of the semi-chord and leading-edge effects might become relevant, (ii) $\mu = 3.71$ representing the dominant peak in the spectrum, and (iii) $\mu_0 = 10.0$ where the spectrum from the pressure probe above the airfoil shows a considerably higher amplitude than the spectrum below the airfoil, implying that an additional noise source might be present. The frequency resolution of the spectra is $\Delta\mu_0 = 4.8 \times 10^{-2}$.

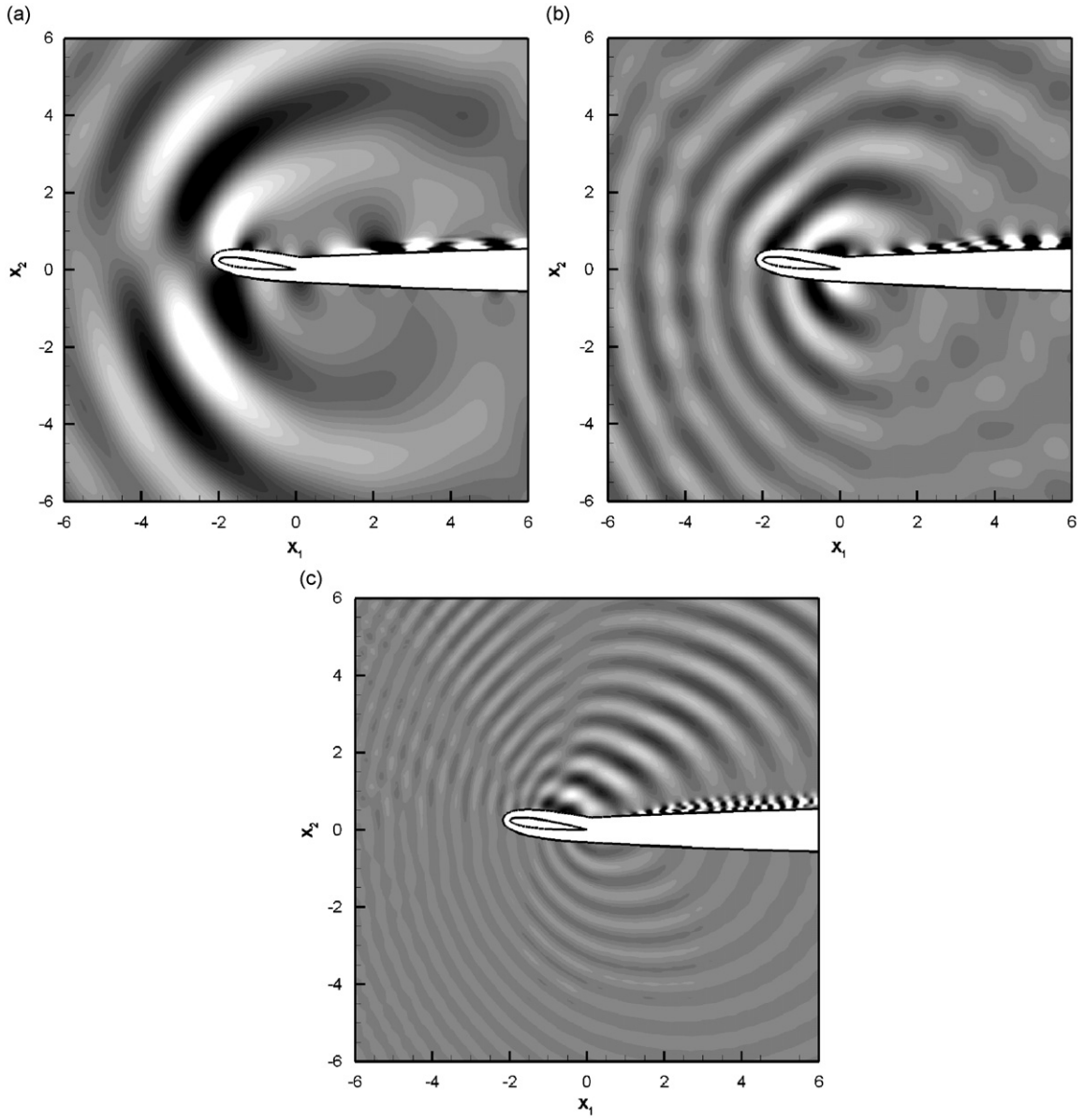

Fig. 11. Contours of real part of acoustic pressure for $\mu_0 = 2.0$ (a), $\mu_0 = 3.71$ (b), and $\mu_0 = 10.0$ (c); 21 levels in range $[-2 \times 10^{-3}; 2 \times 10^{-3}]$; $\alpha = 7^{\circ}$.

In Fig. 11 the real part of the acoustic pressure is shown for the three representative frequencies. In order to generate information for the acoustic field in the frequency domain, the entire time-series of the spanwise plane was required. To reduce the size of data stored to disk, the time-series of pressure was stored only for the acoustic field and not the hydrodynamic field, which contains the majority of the total number of grid points. Therefore, the hydrodynamic field is removed from Figs. 11(a)–(c). For clarity, the airfoil surface is denoted by a solid line.

At $\mu_0 = 2.0$ and 3.71, sound waves are observed emanating from the trailing edge above and below the airfoil in opposite phase, suggesting that the trailing edge is the main noise source for these two frequencies. In contrast, for $\mu_0 = 10.0$, sound waves, in addition to those generated by the trailing edge, can be observed propagating in the downstream direction, originating above the airfoil upstream of the trailing edge. These additional sound waves are most likely responsible for the higher amplitudes in the spectrum of the pressure

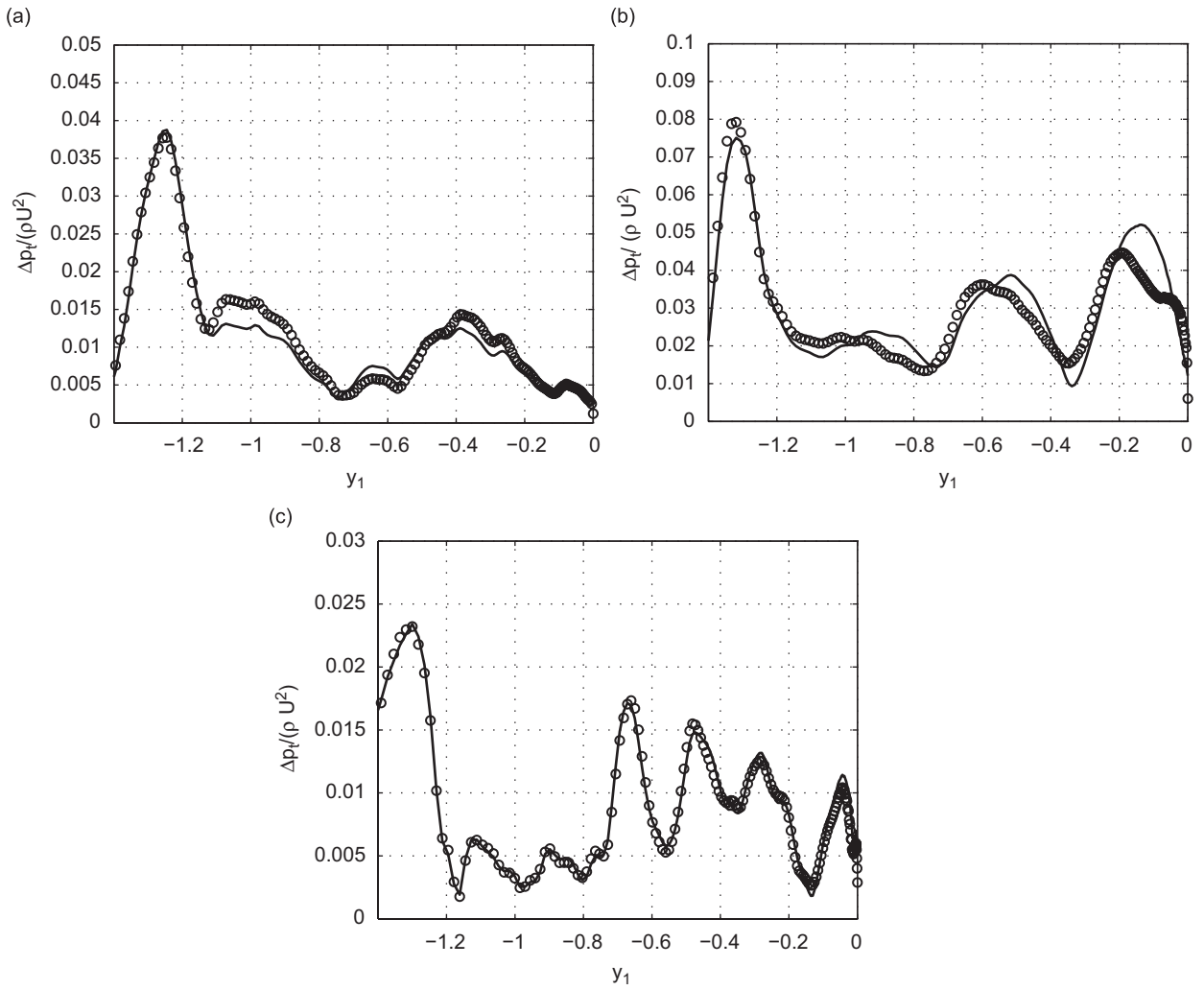

Fig. 12. Magnitude of total surface pressure difference for $\mu_0 = 2.0$ (a), $\mu_0 = 3.71$ (b), and $\mu_0 = 10.0$ (c); (—) $\Delta p_t = p_{\text{top}} - p_{\text{bot}}$, (○) $\Delta p_t = (1 + H_S)p_i$; $U_c = 0.7$, $\alpha = 7^\circ$.

probe above the airfoil. A fully three-dimensional study of a NACA-0012 airfoil at incidence [31] has revealed that the unanticipated additional noise sources on the suction side of the airfoil are not a consequence of the coherent flow patterns that are enforced by conducting a two-dimensional simulation. Even though the flow transitions to turbulence in the separated shear layer in the three-dimensional case, additional noise sources were found on the suction side of the airfoil for several frequencies. It is also noteworthy that the amplitudes of the sound waves for the lower two frequencies are similar to the $\alpha = 5^\circ$ case. This is unexpected when one takes into account the magnitude of the surface pressure difference at the same time, shown in Figs. 12(a) and (b). The amplitudes of Δp_t are lower by up to a factor of three for all frequencies when compared to the case at lower incidence. For trailing-edge noise, it is assumed that the radiated noise is directly proportional to the surface pressure difference. Hence, a considerably lower level of Δp_t would suggest smaller amplitudes of the acoustic pressure. As this is not the case for $\mu_0 = 2.0$ and 3.71, two possible reasons are proposed. Firstly, nonlinear interaction of various frequency components might be responsible for the large acoustic pressure amplitudes, i.e. the acoustic pressure generated at the trailing edge for a specific frequency μ_0 is superposed with the noise generated by the nonlinear interaction of other frequencies resulting in the same frequency μ_0. This, of course, would lead to a difference in the directivity pattern which will be discussed below. Secondly, the vortices on the suction side pass over the trailing edge at a greater distance due to the higher angle of

attack, inducing a smaller surface pressure difference. This, however, would imply that the acoustic noise is produced directly by the vortices and not the surface pressure difference, which would be in agreement with the observations made in simulations over a NACA-0012 airfoil with a rounded trailing edge at $\alpha = 8^\circ$ [15].

In general the surface pressure difference distribution over the chord is similar to the $\alpha = 5^\circ$ case in that there is a peak at $y_1 \approx -1.3$ which denotes the shedding location of the vortices on the suction side. However, the chordwise distribution is not the same for all frequencies. For $\mu_0 = 2.0$ the amplitude of Δp_t decreases over chord, in contrast to the two higher amplitudes shown where the amplitude increases, only to significantly drop in the vicinity of the trailing edge. The small amplitude of the surface pressure difference at the trailing edge for all frequencies again suggests that the Kutta condition is a reasonable assumption even for viscous flows over airfoils.

The surface pressure jump function is evaluated using the incident pressure field computed according to Eq. (7) for all frequencies and shown in Fig. 12. For the frequency of the vortex shedding on the suction side of

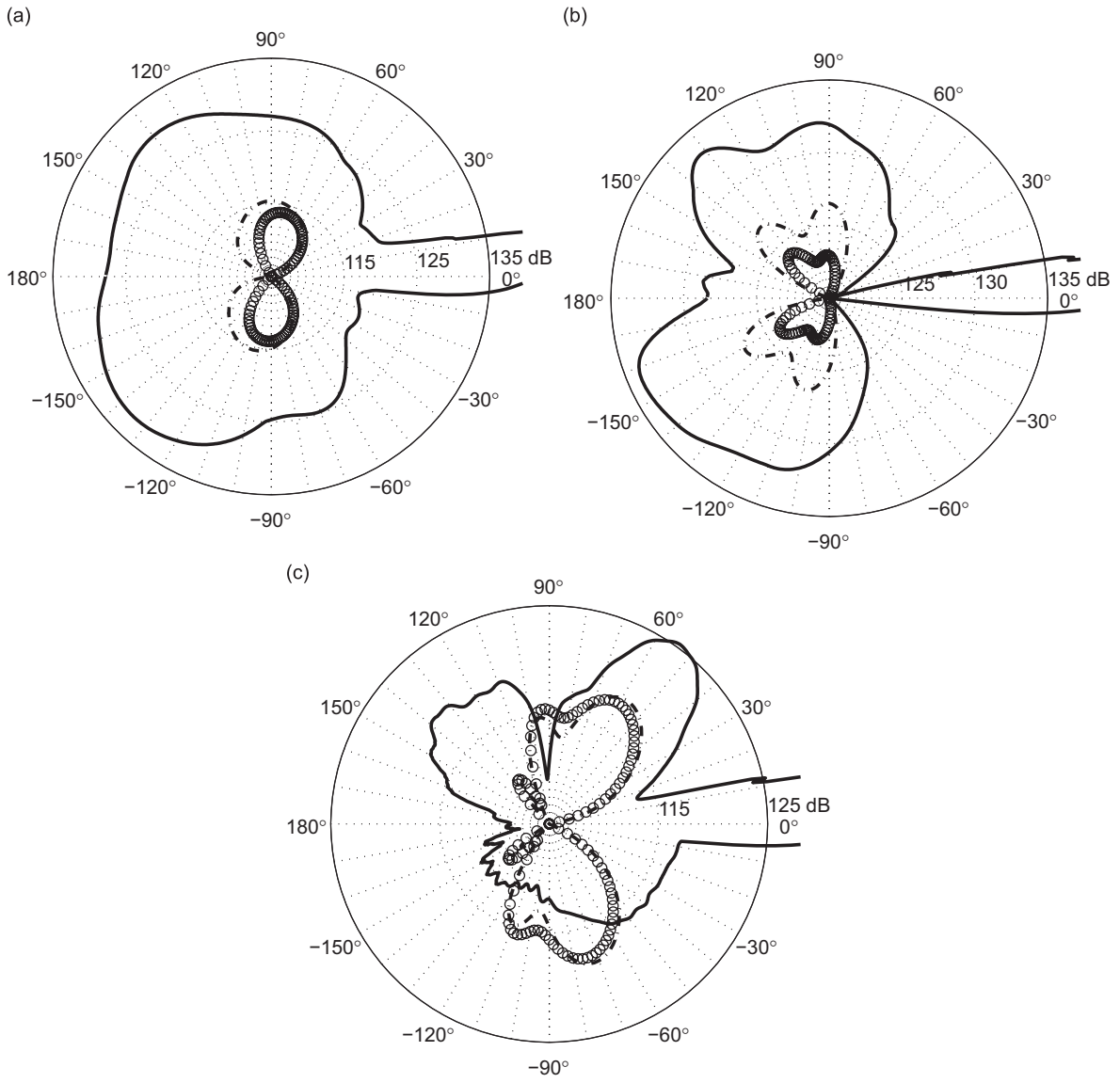

Fig. 13. Magnitude of acoustic pressure at $R_d = 4$ for $\mu_0 = 2.0$ (a), $\mu_0 = 3.71$ (b), and $\mu_0 = 10.0$ (c); $(- \cdot -)$ $\Delta p_t = p_{\text{top}} - p_{\text{bot}}$, $(\circ)$ $\Delta p_t = (1 + H_S)p_i$, (—) acoustic pressure from DNS; $U_c = 0.7$, $\alpha = 7^\circ$.

the airfoil, an extra peak is predicted close to the trailing edge leading to a significant phase shift of all other peaks. This suggests that the performance of the response function deteriorates when large vortices with significant spanwise coherence pass the trailing edge. However, at the lowest frequency shown the agreement with the DNS data is better and at $\mu_0 = 10.0$ the predicted surface pressure difference agrees well with the DNS solution. In the case of fully three-dimensional simulations the flow becomes less correlated in the spanwise direction and the surface pressure jump function appears to perform slightly better, albeit its performance deteriorates for lower frequencies [31].

Finally, the directivity of the acoustic pressure is shown for each frequency in Fig. 13. As was expected from the above discussion, the amplitudes of the acoustic pressure predicted by both the acoustic analogy and the modified theory of Amiet are significantly lower (5–10 dB) than those obtained directly from DNS. For the frequency of the vortex shedding on the suction side of the airfoil, $\mu_0 = 3.71$, the shape of the directivity agrees fairly well with the DNS data. However, for the other two frequencies shown, the agreement is poor. For these two frequencies, the DNS data also display disparate directivities above and below the airfoil, implying that the radiated sound is not due to the classical trailing-edge noise mechanisms. At $\mu_0 = 10.0$ the downstream pointing lobe on the top side is a result of the sound waves originating on the suction side upstream of the trailing edge as observed in Fig. 11(c). It can be speculated that the noise is generated by the vortices directly as proposed by Tam and Ju [15] for a NACA-0012 airfoil at $\alpha = 8^\circ$. Another observation can be made which supports the above hypothesis. At lower incidence, the sound level was very small directly upstream of the airfoil (for seven degrees above and below the airfoil chord line) due to the dipole-nature of the trailing-edge noise (see Figs. 4, 5, 8, and 10). Here at $\alpha = 7^\circ$, the amplitudes of the radiated sound upstream of the extension of the airfoil chord line are not significantly decreased, in particular for the low frequency $\mu_0 = 2.0$. The high noise level in the upstream extension of the chord line suggests the presence of additional noise sources upstream of the trailing edge and/or away from the surface. The approach of predicting the airfoil self-noise as a function of the surface pressure difference only therefore appears to not be applicable for all frequencies at higher angles of attack. This implies that for certain flow conditions, the approximation made in Amiet's classical trailing-edge theory to neglect volume sources in the flow is not applicable. This conjecture could be validated by using Kirchhoff surfaces on and away from the airfoil surface to predict the far-field noise. However, this approach is not without problems as there are issues with how to close the Kirchhoff surface in the wake region [32].

5. Summary

Direct numerical simulations were conducted of compressible flow at $M = 0.4$ over symmetric NACA airfoils with $\alpha = 0^\circ$, 5°, and 7°. The Reynolds number based on chord was specified as $Re = 5 \times 10^4$. Spectra of the surface pressure difference at the trailing edge and of pressure probes above and below the airfoil reveal distinct tones for the $\alpha = 0^\circ$ and 5° cases, and a broadband-like behavior for the airfoil at $\alpha = 7^\circ$. The tones are linked to the frequencies of the wake shedding and forced Tollmien–Schlichting (T–S) waves at zero incidence, and to the frequency of the vortex shedding on the suction side and its higher harmonics at $\alpha = 5^\circ$. At $\alpha = 7^\circ$, the dominant peak in the spectrum can be attributed to the vortex shedding caused by the laminar separation bubble.

For the wake frequency of the NACA-0012 airfoil at zero incidence the surface pressure difference is induced by the unsteady wake, i.e. the top and bottom sides are of opposite phase. As a result, the incident pressure field is zero and a doubling of the top or bottom surface yields the total surface pressure difference which reaches a peak at the trailing edge, i.e. the Kutta condition is not satisfied. This is in contrast to all other cases investigated where the Kutta condition appears to be a valid approximation. Using the acoustic analogy, the acoustic pressure can be predicted to within approximately 2 dB as a function of surface pressure difference, in spite of the finite thickness geometry of the airfoil and viscous effects not being accounted for by the flat-plate theory. The fairly good prediction of the radiated noise using the trailing-edge noise theory also implies that noise is generated by the induced pressure difference on the airfoil surface and not the vortices in the wake as has been previously suggested [15].

In the case of T–S waves convecting over the airfoil and passing over the trailing edge, it is demonstrated that Amiet's surface pressure jump function provides an accurate prediction of the scattered pressure field.

However, in the NACA-0012 case an unexpected change of phase is needed to be accounted for to obtain an accurate representation of the total surface pressure difference, and consequently the sound radiation. It is proposed that the presence of a wake with a frequency other than the forcing frequency in the NACA-0012 case leads to flow oscillating around the trailing edge at the wake frequency, causing a recirculation region in the mean flow downstream of the trailing edge. This was not the case for the airfoils with a smaller trailing-edge angle (NACA-0006 and NACA-0008), where a lack of a second peak in the spectrum indicates that the wake frequency locks into the forcing frequency and no mean reverse velocity is present in the wake.

At $\alpha = 5^\circ$ the surface pressure jump function yields a good prediction of the total surface pressure difference in terms of peak locations, hence the directivity of the acoustic pressure evaluated using the modified theory of Amiet compares favorably with the DNS data. Because the amplitude of the total surface pressure difference is underpredicted, the amplitude of the acoustic pressure is predicted within 5 dB of the DNS data. For increasing incidence, the performance of the surface pressure jump function deteriorates and a considerable 'phase error' occurs when comparing the predicted surface pressure difference with the DNS data at the vortex shedding frequency. This results in a poor prediction of the acoustic pressure using the modified theory of Amiet, and suggests that the response function is not suited to cases where large vortices with a high spanwise coherence pass the trailing edge. In addition, high noise levels in the upstream extension of the airfoil chord line and strongly asymmetric directivity distributions above and below the airfoil for $\alpha = 7^\circ$ suggest that the radiated sound is not only due to classical trailing-edge noise mechanisms. It is speculated that in this case the noise is generated directly by the vortices on the suction side, as previously proposed [15]. In general, it appears that the modified theory of Amiet is suitable for finite thickness airfoils at only moderate angles of attack (up to $\alpha = 5^\circ$ in this study). Predicting airfoil self-noise based on the surface pressure difference alone appears not to be applicable for all frequencies at higher angles of attack. It is suggested that for certain cases volume sources cannot be neglected, as is done in Amiet's classical trailing-edge theory.

Acknowledgments

This work was supported by the DTI under the MSTTAR DARP programme. Computer time was provided by the UK turbulence consortium under EPSRC Grant EP/D044073/1.

References

[1] J. Ffowcs Williams, L. Hall, Aerodynamic sound generation by turbulent flow in the vicinity of a scattering half plane, *Journal of Fluid Mechanics* 40 (4) (1970) 657–670.
[2] M.J. Lighthill, On sound generated aerodynamically I. General theory, *Proceedings of the Royal Society of London, Series A: Mathematical and Physical Science* 211A (1107) (1952) 564–587.
[3] M.J. Lighthill, On sound generated aerodynamically II. Turbulence as a source of sound, *Proceedings of the Royal Society of London, Series A: Mathematical and Physical Science* 222 (1148) (1952) 1–32.
[4] M.S. Howe, A review of the theory of trailing edge noise, *Journal of Sound and Vibration* 61 (3) (1978) 437–465.
[5] T. Brooks, T. Hodgson, Trailing edge noise prediction from measured surface pressures, *Journal of Sound and Vibration* 78 (1) (1981) 69–117.
[6] R. Amiet, Noise due to turbulent flow past a trailing edge, *Journal of Sound and Vibration* 47 (3) (1976) 387–393.
[7] R.W. Paterson, R.K. Amiet, Acoustic radiation and surface pressure characteristics of an airfoil due to incident turbulence, *13th AIAA Aeroacoustics Conference*, AIAA paper 76-57, Palo Alto, CA.
[8] I. Evers, N. Peake, On sound generation by the interaction between turbulence and a cascade of airfoils with non-uniform mean flow, *Journal of Fluid Mechanics* 463 (2002) 25–52.
[9] R.W. Paterson, P.G. Vogt, M.R. Fink, C.L. Munch, Vortex noise of isolated airfoils, *Journal of Aircraft* 10 (5) (1973) 296–302.
[10] R.H. Schlinker, R.K. Amiet, M.R. Fink, Vortex noise from nonrotating cylinders and airfoils, AIAA Paper 1976-81.
[11] H. Arbey, J. Bataille, Noise generated by airfoil profiles placed in a uniform laminar-flow, *Journal of Fluid Mechanics* 134 (1983) 33–47.
[12] E. Nash, M. Lowson, A. McAlpine, Boundary-layer instability noise on aerofoils, *Journal of Fluid Mechanics* 382 (1999) 27–61.
[13] G. Desqesnes, M. Terracol, P. Sagaut, Numerical investigation of the tone noise mechanism over laminar airfoils, *Journal of Fluid Mechanics* 591 (2007) 155–182.
[14] M. Roger, S. Moreau, A. Guédel, Vortex-shedding noise and potential-interaction noise modelling by a reversed Sear's problem, *12th AIAA/CEAS Aeroacoustics Conference* (*27th AIAA Aeroacoustics Conference*), AIAA paper 2006-2607, Cambridge, MA.

[15] C.K.W. Tam, H. Ju, Numerical simulation of the generation of airfoil tones at a moderate Reynolds number, *12th AIAA/CEAS Aeroacoustics Conference* (*27th AIAA Aeroacoustics Conference*), AIAA Paper 2006-2502, Cambridge, MA.
[16] P.F. Mish, W.J. Devenport, An experimental investigation of unsteady surface pressure on an airfoil in turbulence–part 1: effect of mean loading, *Journal of Sound and Vibration* 296 (2006) 417–446.
[17] S. Moreau, M. Roger, Effect of airfoil aerodynamic loading on trailing-edge noise sources, *AIAA Journal* 43 (1) (2005) 41–52.
[18] R.D. Sandberg, N.D. Sandham, P.F. Joseph, Direct numerical simulations of trailing-edge noise generated by boundary-layer instabilities, *Journal of Sound and Vibration* 304 (3–5) (2007) 677–690.
[19] F.M. White, *Viscous Fluid Flow*, McGraw-Hill, New York, 1991.
[20] M. Wei, J. Freund, A noise-controlled free shear flow, *Journal of Fluid Mechanics* 546 (2006) 123–152.
[21] M.E. Goldstein, *Aeroacoustics*, first ed., McGraw-Hill, New York, 1976.
[22] R. Amiet, High-frequency thin airfoil theory for subsonic flow, *AIAA Journal* 14 (8) (1976) 1076–1082.
[23] R. Amiet, Effect of the incident surface pressure field on noise due to turbulent flow past a trailing edge, *Journal of Sound and Vibration* 57 (2) (1978) 305–306.
[24] M. Roger, S. Moreau, Broadband self-noise from loaded fan blades, *AIAA Journal* 42 (3) (2004) 536–544.
[25] M. Roger, S. Moreau, Back-scattering correction and further extensions of Amiet's trailing-edge noise model, part 1: theory, *Journal of Sound and Vibration* 286 (2005) 477–506.
[26] N. Sandham, Q. Li, H. Yee, Entropy splitting for high-order numerical simulation of compressible turbulence, *Journal of Computational Physics* 178 (2002) 307–322.
[27] R.D. Sandberg, N.D. Sandham, Nonreflecting zonal characteristic boundary condition for direct numerical simulation of aerodynamic sound, *AIAA Journal* 44 (2) (2006) 402–405.
[28] L.E. Jones, R. Sandberg, N. Sandham, Direct numerical simulations of forced and unforced separation bubbles on an airfoil at incidence, *Journal of Fluid Mechanics* 602 (2008) 175–207.
[29] Z.W. Hu, C.L. Morfey, N.D. Sandham, Wall pressure and shear stress spectra from direct simulations of channel flow, *AIAA Journal* 44 (7) (2006) 1541–1549.
[30] R.D. Sandberg, N.D. Sandham, Direct numerical simulation of turbulent flow past a trailing edge and the associated noise generation, *Journal of Fluid Mechanics* 596 (2008) 353–385.
[31] R.D. Sandberg, L.E. Jones, N.D. Sandham, Direct numerical simulations of noise generated by turbulent flow over airfoils, *14th AIAA/CEAS Aeroacoustics Conference* (*29th AIAA Aeroacoustics Conference*), AIAA Paper 2008-2861, Vancouver, Canada.
[32] B. Singer, K. Brentner, D. Lockard, G. Lilley, Simulation of acoustic scattering from a trailing edge, *Journal of Sound and Vibration* 230 (3) (2000) 541–560.